12th International Symposium on Turbulence and Shear Flow Phenomena (TSFP12)
Osaka, Japan (Online), July 19-22, 2022

FEEDBACK CONTROL EFFECT IN TURBULENT CHANNEL FLOW WITH A BUMP BY MEANS OF DIRECT NUMERICAL SIMULATION

Yusuke OKOCHI
Department of Mechanical Engineering
Keio University
Hiyoshi 3-14-1, Kohoku-ku, Yokohama, Japan
y.okochi@keio.jp

Yusuke NABAE
Department of Mechanical Engineering
Keio University
Hiyoshi 3-14-1, Kohoku-ku, Yokohama, Japan
yusuke.nabae@kflab.jp

Koji FUKAGATA
Department of Mechanical Engineering
Keio University
Hiyoshi 3-14-1, Kohoku-ku, Yokohama, Japan
fukagata@mech.keio.ac.jp

ABSTRACT

We investigate the effect of feedback control in a turbulent channel flow with a bump by means of direct numerical simulation (DNS). In this study, the opposition control proposed by Choi *et al.* (1994), which is the simplest feedback control method, is applied and the detection plane is set at about 15 wall units from the wall. Two bulk Reynolds numbers, $\mathrm{Re}_b = 5600$ and 12600, and two different bump heights, $h^+ \approx 20$ and 40, are considered. According to the DNS results, although the pressure drag is hardly changed, the total drag is decreased due to reduction of the friction drag in both cases of $h^+ \approx 20$ and 40. In addition, the control effect decreases as the bump height increases due to enhancement of the flow separation. The control effect decreases also as the Reynolds number increases.

INTRODUCTION

Although reduction of flow drag is of great importance for energy savings, there are few practical flow control methods for friction drag reduction. Therefore, development of practical flow control methods has been strongly desired.

The opposition control proposed by Choi *et al.* (1994) is the simplest feedback control scheme, which suited to study the effect of attenuation of quasi-streamwise vortices in the region near the wall. In this control method, the control input on the walls is determined based on the velocity in the detection plane. Choi *et al.* (1994) achieved 25% drag reduction in a relatively low-Reynolds-number turbulent plane channel flow by means of direct numerical simulation (DNS). Hammond *et al.* (1998) optimized the location of the detection plane in the opposition control, and the drag reduction rate was found to be maximum when the detection plane was placed about 15 wall units above the wall, i.e., $y^+ \approx 15$.

On the other hand, the effect of feedback control in a turbulent channel flow with a bump has been still unknown due to its complexity, e.g., flow separation. However, investigation of the feedback control effect in a turbulent channel flow with a bump has a crucial importance toward practical implementation of feedback control.

Based on the aforementioned background, the objective of the present study is to investigate the effect of feedback control in a turbulent channel flow with a bump by means of DNS. We apply the opposition control as a representative example of feedback control and investigate its control effect. Then, two different bump heights are considered to investigate the dependence of the drag reduction effect on the bump height. Additionally, the control method is applied at two different bulk Reynolds numbers to investigate the Reynolds number dependence of the control in this flow geometry.

NUMERICAL METHODS

Coordinate system

In order to enable the simulation in the orthogonal coordinate system, the coordinate transformation proposed by Kang & Choi (2000) is applied as follows:

$$x = \xi_1, y = \xi_2(1+\eta) + \eta_l, z = \xi_3, \tag{1}$$

where ξ_1,ξ_2 and ξ_3 denote the streamwise, wall-normal and spanwise directions in the computational space, respectively. Also, $\eta = (\eta_u - \eta_l)/2$ with η_u and η_l denoting the displacement of the upper and lower walls. Following Banchetti *et al.* (2020), who studied the effect of streamwise-travelling waves of spanwise velocity over a bump, η_u and η_l are defined as

$$\eta_u = 0, \tag{2}$$

$$\eta_l = a\exp\left[-\left(\frac{\xi_1 - b}{c}\right)^2\right] + a'\exp\left[-\left(\frac{\xi_1 - b}{c'}\right)^2\right], \tag{3}$$

where a, a', c and c' are the parameters to determine the configuration of the bump. In this study, these parameters are set to $(a,\ a',\ c,\ c') = (0.0505,\ 0.060425,\ 0.2922,\ 0.3847)$,

Table 1. Computational conditions.

	Re_b	$L_1 \times L_2 \times L_3$	$N_1 \times N_2 \times N_3$	$\Delta\xi_1^+$	$\Delta\xi_2^+$	$\Delta\xi_3^+$
Driver	5600	$4\pi \times 2 \times 2\pi$	$256 \times 96 \times 256$	8.8	0.9-6.0	4.4
Main	5600	$4\pi \times 2 \times 2\pi$	$256 \times 96 \times 256$	8.8	0.9-6.0	4.4
Driver	12600	$2\pi \times 2 \times \pi$	$256 \times 192 \times 256$	8.8	0.9-6.0	4.4
Main	12600	$2\pi \times 2 \times \pi$	$256 \times 192 \times 256$	8.8	0.9-6.0	4.4

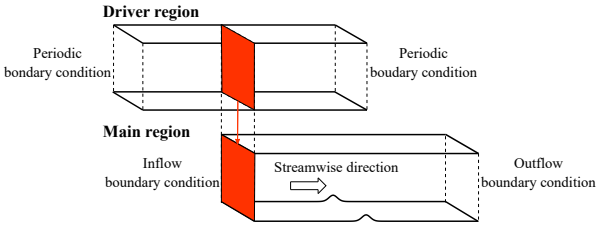

Figure 1. The schematic of the computational domains.

so that the bump height is $h^+ \approx 20$, where $()^+$ denotes the wall unit based on the friction velocity of the uncontrolled flow. For the case of $h^+ \approx 40$, $(a,\ a',\ c,\ c') = (0.1010,\ 0.120850,\ 0.2922,\ 0.3847)$. The bump is located at the center of the channel, i.e., $b = 2\pi$.

Governing equations

The governing equations are the incompressible continuity and Navier-Stokes equations in the boundary-fitted coordinates, i.e.,

$$\frac{\partial u_i}{\partial \xi_i} = -S, \tag{4}$$

$$\frac{\partial u_i}{\partial t} = -\frac{\partial \left(u_i u_j\right)}{\partial \xi_j} - \frac{\partial p}{\partial \xi_i} + \frac{1}{\mathrm{Re}_b}\frac{\partial^2 u_i}{\partial \xi_j \xi_j} - \frac{dP}{d\xi_1}\delta_{i1} + S_i, \tag{5}$$

where S and S_i in Eqs. (4) and (5) denote the additional terms due to the coordinate transformation. All variables are made dimensionless by twice the bulk-mean velocity $2U_b^*$, the channel half-width δ^*, and the fluid density ρ^*. The bulk Reynolds number, $\mathrm{Re}_b = 2U_b^*\delta^*/\nu^*$ is 5600 or 12600, which corresponds to the friction Reynolds number of $\mathrm{Re}_\tau = 180$ and 360, respectively, in the uncontrolled flow. Here, the superscript $*$ denotes dimensional quantities. All simulations are conducted under the constant flow rate condition.

Numerical conditions

The computational domain consists of two regions, i.e., a driver region without a bump and a main region with a bump as shown in Figure 1. In the driver region, the periodic boundary condition is applied in the streamwise (ξ_1) and spanwise (ξ_3) directions, and the no-slip condition is applied on both walls. In the main region, the inflow and outflow boundary conditions are applied in the streamwise direction and the periodic boundary condition is applied in the spanwise direction. On the lower wall ($\xi_2 = 0$), the following velocity, i.e.,

$$v(\xi_1, 0, \xi_3) = -v(\xi_1, \xi_{2,d}, \xi_3) + \overline{v(\xi_1, \xi_{2,d}, \xi_3)}^{\xi_3}, \tag{6}$$

Table 2. Each drag coefficient in the uncontrolled and controlled cases and the reduction rate of the drag coefficient when $h^+ \approx 20$ and $\mathrm{Re}_b = 5600$.

	Uncontrolled	Contolled	R_D
$C_{Df,u}[\times 10^{-3}]$	8.08	6.07	24.9%
$C_{Df,l}[\times 10^{-3}]$	7.99	5.95	25.5%
$C_{Dp,l}[\times 10^{-3}]$	1.20	1.17	2.5%
$C_D[\times 10^{-3}]$	17.27	13.19	23.6%

is imposed in both domains. Note that in order to make the total mass flux from the wall zero, the second term on the right-hand-side in Eq. (6) is added. In this study, the detection plane is set to $\xi_{2,d}^+ \approx 15$. The DNS code is based on that of Fukagata *et al.* (2006) and the code for the driver domain is based on that of a spatially developing turbulent boundary layer flow extended by Kametani & Fukagata (2011). The computational conditions are shown in Table 1.

Drag coefficients

The total drag coefficient, C_D can be decomposed into the friction drag, C_{Df} and the pressure drag, C_{Dp}, i.e.,

$$C_D = C_{Df,u} + C_{Df,l} + C_{Dp,l}, \tag{7}$$

where $(\cdot)_u$ and $(\cdot)_l$ denote quantities on the upper and lower walls, respectively. Similar to Mori *et al.* (2017), the friction and pressure drags can be computed as follows:

$$C_{Df} = \frac{1}{(1/2)\rho^* U_b^{*2}} \frac{1}{L_1 L_3} \int_0^{L_1}\int_0^{L_3} \boldsymbol{e}_1 \cdot \boldsymbol{\tau}^* \cdot \boldsymbol{n}\, dx_3 dx_1, \tag{8}$$

$$C_{Dp} = \frac{1}{(1/2)\rho^* U_b^{*2}} \frac{1}{L_1 L_3} \int_0^{L_1}\int_0^{L_3} \boldsymbol{e}_1 \cdot (-p_w^* \boldsymbol{I}) \cdot \boldsymbol{n}\, dx_3 dx_1, \tag{9}$$

where $\boldsymbol{\tau}^*$, p_w, $\boldsymbol{e}_1$ and $\boldsymbol{n}$ represent the viscous stress tensor, the pressure on the wall, the streamwise unit vector and the wall-normal unit vector, respectively.

RESULTS AND DISCUSSION

Effects of the opposition control

For the bump height of $h^+ \approx 20$ at $\mathrm{Re}_b = 5600$, the total drag reduction rate obtained is 23.6%. Each component of the drag coefficients in the uncontrolled and controlled cases and the reduction rate by the control are shown in Table 2.

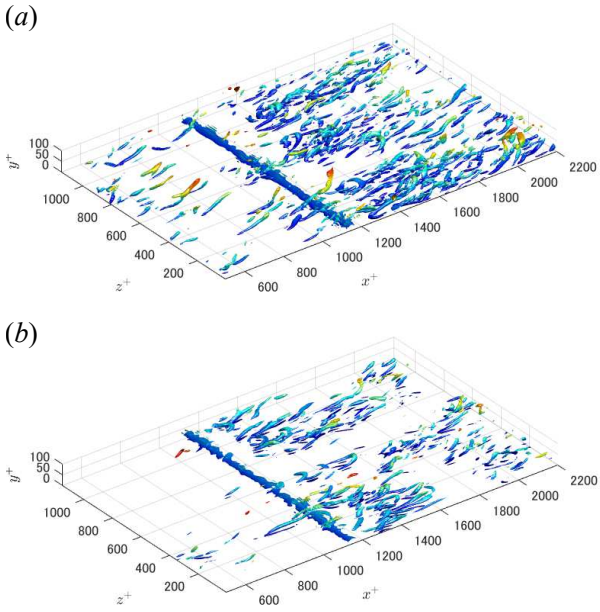

Figure 2. Visualization of vortical structures in the uncontrolled and controlled cases (threshhold, $Q^+ = -0.07$; color, the wall-normal coordinate in the real space, y^+): (a) uncontrolled case; (b) controlled case.

Focusing on the contributions from the friction drag and the pressure drag, the friction drag decreases by 25.5% and the pressure drag slightly decreases by 2.5%. The friction drag reduction rate in the present study is almost the same as that in the case without a bump, i.e., 25% (Hammond *et al.*, 1998) on both walls. Thus, existence of a bump hardly decreases the friction drag reduction effect.

Figure 2 shows the visualization of vortical structures identified by the second invariant of velocity gradient tensor, Q (Hunt *et al.*, 1988). In the upstream region of the bump ($x^+ < 1000$), vortical structures are significantly suppressed by the control. This trend is basically similar to that in the case without a bump (Hammond *et al.*, 1998). Conversely, vortical structures around and rear the bump ($1200 < x^+ < 1400$) are enhanced and turbulence is activated by the control.

Figure 3 shows a comparison of streamwise velocity fields around and rear the bump. The white line in Figure 3 represents $u = 0$. In the region behind the bump, streamwise velocity is negative, indicating that the flow is separated from the lower wall. Compared to the uncontrolled case, the reattachment position in the controlled case shifts further downstream as shown in Figure 3. It is clearly observed that the flow separation is enhanced downstream by the control.

Figure 4 shows the friction drag and the pressure on the lower wall in the streamwise direction. As shown in Figure 4 (a), the friction drag is reduced by the control in the wide region except for the region just behind the bump center where the flow is separated. On the other hand, the friction drag behind the bump ($1200 < x^+ < 1400$) is not suppressed by the control. Therefore, it can be suggested that the effect of the friction drag reduction by the opposition control is hardly obtained in the region where the flow separation occurs. Also, the pressure on the lower wall is not almost modified by the control in the whole region of the channel.

As shown in Figure 5, similar to the case without a bump (Hammond *et al.*, 1998), streak structures lined up in the spanwise direction at $\xi_2^+ \approx 8$ are suppressed in the regions where

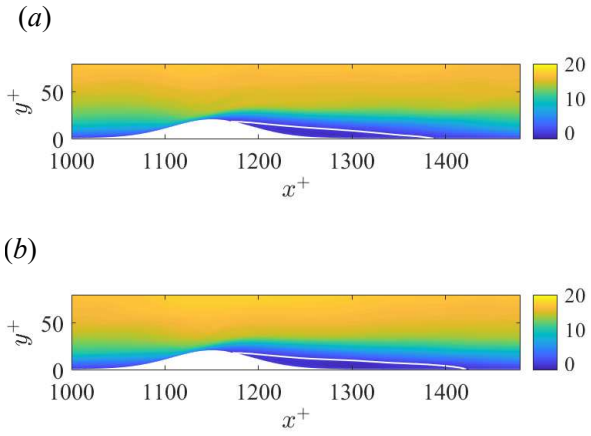

Figure 3. Streamwise velocity in the region around and rear the bump in the case of $h^+ \approx 20$ at $\mathrm{Re}_b = 5600$: (a) uncontrolled case; (b) controlled case.

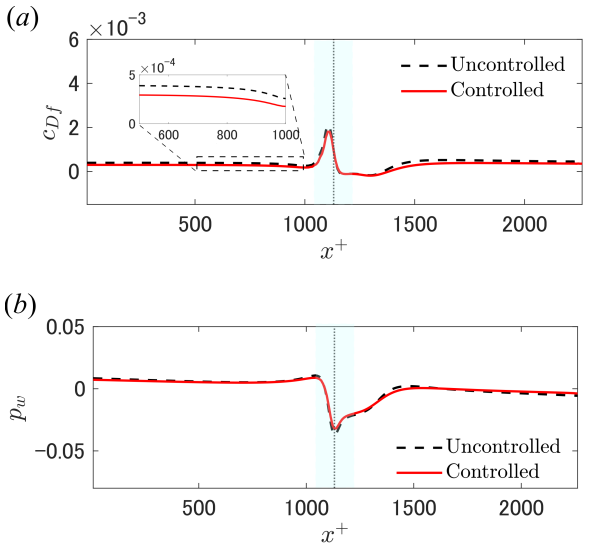

Figure 4. The friction drag coefficient and the pressure on the lower wall in the uncontrolled and controlled cases of $h^+ \approx 20$ at $\mathrm{Re}_b = 5600$ (colored area shows the region where the bump exists): (a) the friction drag coefficient; (b) pressure on the lower wall.

the friction drag reduction is achieved ($x^+ < 1000$, $x^+ > 1400$). Since the suppression of the streak structures was observed also in the case without a bump (Hammond *et al.*, 1998), it is implied that the mechanism of the friction drag reduction in this study is basically similar to the case without a bump. On the other hand, the streak structures just behind the bump ($1200 < x^+ < 1400$) are weak even in the uncontrolled case, so that the control effect just behind the bump is little.

The Reynolds shear stress (RSS) at four different locations, i.e., upstream ($x^+ \approx 1050$), the top ($x^+ \approx 1150$), downstream ($x^+ \approx 1250$) of the bump and rear the bump ($x^+ \approx 2000$) is shown in Figure 6. Except for the downstream region of the bump ($x^+ \approx 1250$), RSS shifts away from the wall, resulting in suppression of RSS near the wall. This trend is similar to the case without a bump. On the other hand, the RSS in the region near the wall is hardly suppressed at $x^+ \approx 1250$, indicating that the flow separation vanishes the control effect behind the bump.

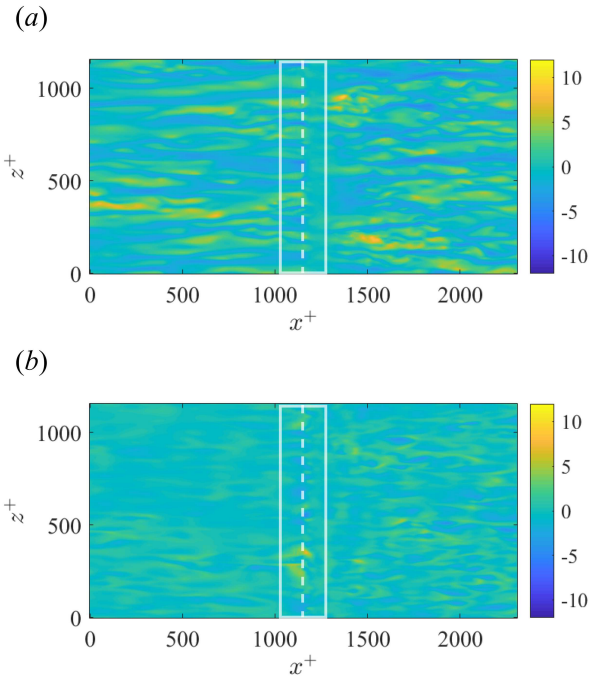

Figure 5. Streamwise velocity fluctuation at $\xi_2^+ \approx 8$ in the uncontrolled and controlled cases of $h^+ \approx 20$ at $\mathrm{Re}_b = 5600$: (a) uncontrolled case; (b) controlled case. Solid white line, the bump; dashed white line, the top of the bump.

When the opposition control is applied to a turbulent channel flow with a bump, the friction drag reduction effect is confirmed in the wide region except for the downstream of the bump where the flow is separated. On the other hand, it is also confirmed that the opposition control has a small effect on the pressure drag, and the flow separation is enhanced. On average, in the case of $h^+ \approx 20$, the total drag is reduced because the friction drag, which accounts for a large amount of the total drag, is reduced by the control.

Dependence of the control effect on the bump height

In order to investigate the dependence of the drag reduction effect on the bump height, the opposition control is applied in the case where the bump height is doubled, i.e., $h^+ \approx 40$. Each drag coefficient in the uncontrolled and controlled cases and the reduction rate of the drag coefficient when $h^+ \approx 40$ and $\mathrm{Re}_b = 5600$ are shown in Table 3. Similar to the case of $h^+ \approx 20$, the friction drag on both walls is decreased, and the pressure drag is slightly decreased. However, the friction drag reduction rates on both walls decrease and the pressure drag increases as the height of the bump increases. Thus, compared to the case of $h^+ \approx 20$, the total drag reduction rate becomes small, i.e., $R_D = 15.0\%$.

The friction drag coefficient and the pressure on the lower wall are shown in Figure 7. The friction drag is reduced in the upstream region of the bump ($x^+ < 1000$). This can be observed also in the case of $h^+ \approx 20$. On the other hand, unlike the case of $h^+ \approx 20$, the friction drag is reduced also in the downstream region of the bump ($x^+ \approx 1500$). Streamwise and wall-normal velocities at $x^+ \approx 1500$ where the friction drag is reduced are shown in Figure 8. As shown in Figure 8 (a), the negative streamwise velocity near the lower wall is enhanced by the control, and it is clear that the flow separation is en-

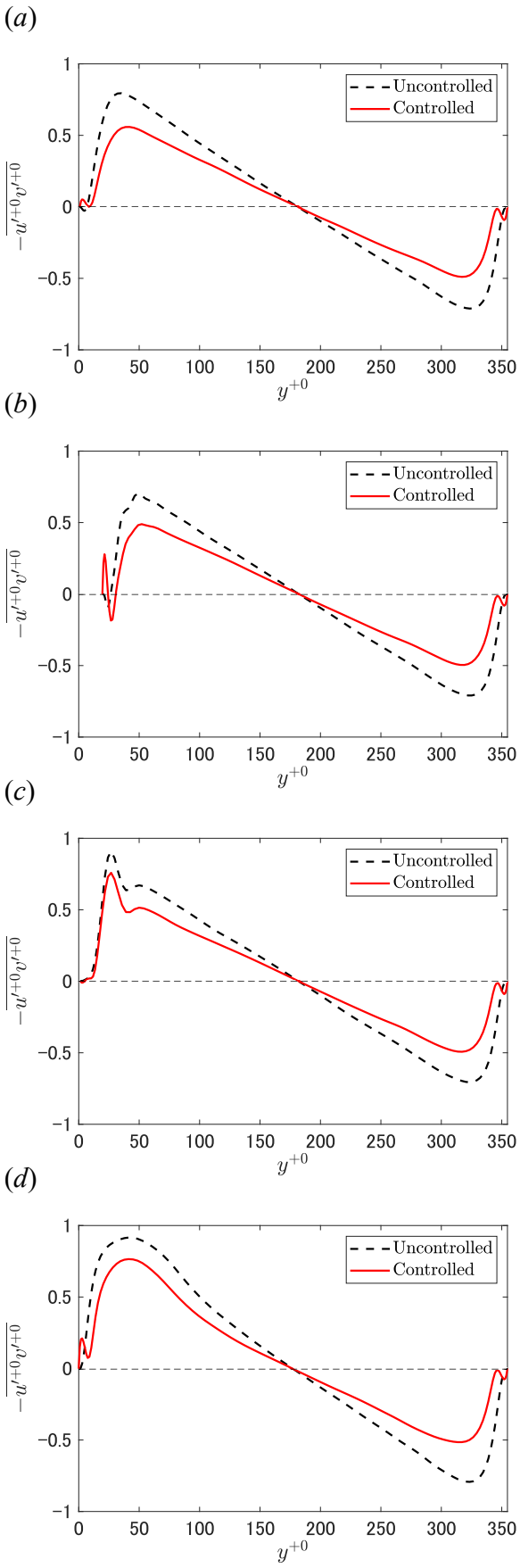

Figure 6. Comparison of Reynolds shear stress in the case of $h^+ \approx 20$ at $\mathrm{Re}_b = 5600$: (a) upstream ($x^+ \approx 1050$); (b) top ($x^+ \approx 1150$); (c) downstream ($x^+ \approx 1250$); (d) the region rear the bump ($x^+ \approx 2000$).

Table 3. Each drag coefficient in the uncontrolled and controlled cases and the reduction rate of the drag coefficient when $h^+ \approx 40$ and $\mathrm{Re}_b = 5600$.

	Uncontrolled	Contolled	R_D
$C_{Df,u}[\times 10^{-3}]$	8.22	6.44	21.6%
$C_{Df,l}[\times 10^{-3}]$	7.71	6.21	19.4%
$C_{Dp,l}[\times 10^{-3}]$	6.47	6.39	1.2%
$C_D[\times 10^{-3}]$	22.40	19.04	15.0%

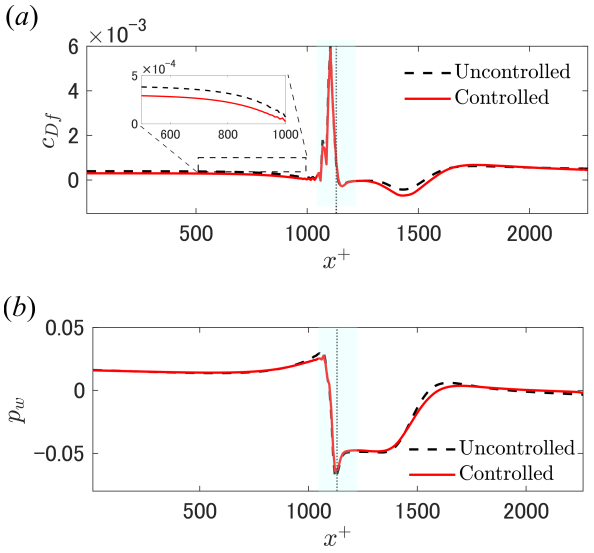

Figure 7. The friction drag coefficient and the pressure on the lower wall in the uncontrolled and controlled cases of $h^+ \approx 40$ at $\mathrm{Re}_b = 5600$ (colored area shows the region where the bump exists): (a) the friction drag coefficient; (b) pressure on the lower wall.

hanced by the control. As shown in Figure 8 (b), negative wall-normal velocity is suppressed by the control and it is also due to enhancement of the flow separation. Therefore, it is suggested that the enhancement of the flow separation leads to the friction drag reduction. It is also noticeable that the friction drag rear the reattachment position ($x^+ > 1600$) is not reduced (Figure 4 (a)) unlike the case of $h^+ \approx 20$. Similar to the case of $h^+ \approx 20$, the control effect for the pressure drag is little.

In sum, although the control reduces the total drag also in the case of $h^+ \approx 40$, the total drag reduction rate is smaller than that in the case of $h^+ \approx 20$. In addition, the flow separation is enhanced by the control in the downstream region of the bump, and it leads to friction drag reduction.

Dependence of the control effect on the Reynolds number

In order to investigate the Reynolds number effect, the opposition control is applied in a flow at a higher Reynolds number, i.e., $\mathrm{Re}_b = 12600$. Here, the bump height is set to $h^+ \approx 20$. Each drag coefficient in the uncontrolled and controlled cases and the reduction rate of the drag coefficient when $h^+ \approx 20$ and $\mathrm{Re}_b = 12600$ are shown in Table 4. The total drag reduction rate is slightly smaller than the case at $\mathrm{Re}_b = 5600$ as shown in Table 2. The friction drag reduction rate on the upper wall decreases as the Reynolds number increases. Ac-

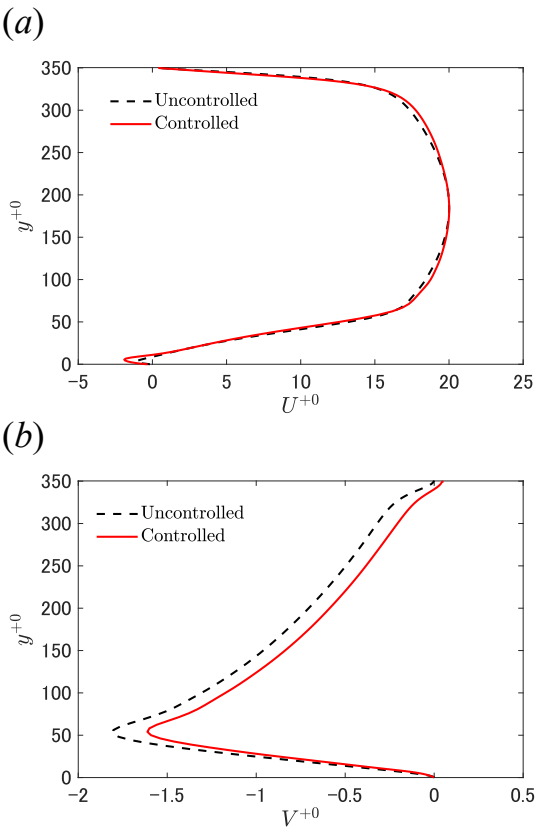

Figure 8. Streamwise and wall-normal velocities at $x^+ \approx 1500$ in the uncontrolled and controlled cases where $h^+ \approx 40$ and $\mathrm{Re}_b = 5600$: (a) streamwise velocity; (b) wall-normal velocity.

Table 4. Each drag coefficient in the uncontrolled and controlled cases and the reduction rate of the drag coefficient when $h^+ \approx 20$ and $\mathrm{Re}_b = 12600$.

	Uncontrolled	Contolled	R_D
$C_{Df,u}[\times 10^{-3}]$	6.55	5.11	21.9%
$C_{Df,l}[\times 10^{-3}]$	6.60	4.94	25.1%
$C_{Dp,l}[\times 10^{-3}]$	0.92	0.93	−1.2%
$C_D[\times 10^{-3}]$	14.07	10.98	21.9%

cording to Chang *et al.* (2002), the friction drag reduction rate by the opposition control decreases as the Reynolds number increases in the case without a bump, and the same trend is observed on the upper wall in the case with the bump. On the other hand, the friction drag reduction rate on the lower wall is similar to that in the case at $\mathrm{Re}_b = 5600$. In other words, the dependence of the control effect on the Reynolds number is different whether a bump exists or not. Focusing on the pressure drag, like the case at $\mathrm{Re}_b = 5600$, the pressure drag is nearly unchanged.

Figure 9 shows the friction drag and the pressure on the lower wall in the streamwise direction. Similar to the case at $\mathrm{Re}_b = 5600$ as shown in Figure 4, reduction of the friction drag can be observed in a wide range except for the vicinity of the bump. In the downstream region of the bump, the friction drag is reduced behind $x^+ \approx 1300$, while the friction drag reduction is observed behind $x^+ \approx 1400$ in the case at

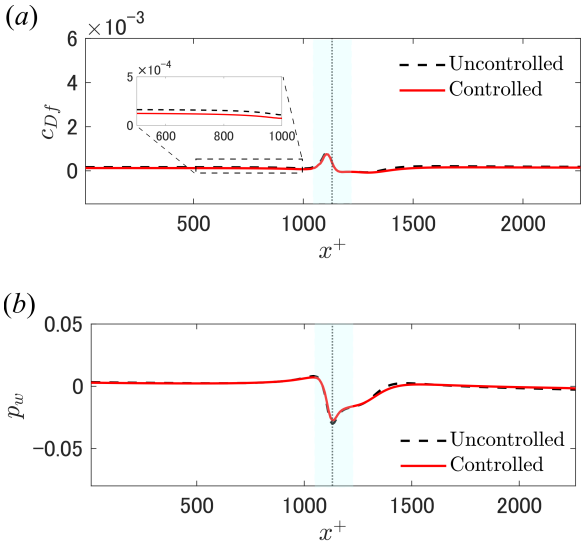

Figure 9. The friction drag coefficient and the pressure on the lower wall in the uncontrolled and controlled cases of $h^+ \approx 20$ at $\mathrm{Re}_b = 12600$ (colored area shows the region where the bump exists): (a) the friction drag coefficient; (b) pressure on the lower wall.

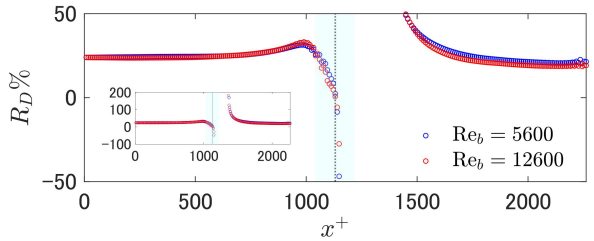

Figure 10. The reduction rate of the local friction drag coefficient at $\mathrm{Re}_b = 5600$ and 12600 (colored area shows the region where the bump exists). Note that the reduction rate is plotted in only the region where the local friction drag coefficient in the uncontrolled case is positive.

$\mathrm{Re}_b = 5600$. It indicates that the separated flow reattatches in more upstream position at a higher Reynolds number and it leads to the larger friction drag reduction rate on the lower wall at $\mathrm{Re}_b = 12600$. In addition, it can be also observed that there is almost no change in the pressure drag by the control, similarly to the case at $\mathrm{Re}_b = 5600$.

Furthermore, in order to investigate the Reynolds number dependence of the friction drag reduction effect by the control in more detail, the local friction drag reduction rates in the cases at $\mathrm{Re}_b = 5600$ and 12600 are shown in Figure 10. In just upstream region of the bump, the friction drag reduction rate at $\mathrm{Re}_b = 5600$ is slightly larger than that at $\mathrm{Re}_b = 12600$. This trend is basically similar to the case without a bump. In the downstream region of the bump, the local reduction rate of the friction drag shifts slightly upstream as Reynolds number increases due to the shift of the reattatchment position. Near the reattachment position, the drag reduction rate is significantly large at both Reynolds numbers.

The total drag reduction rate decreases as the Reynolds number increases, and the local friction drag reduction effect around the bump depends on the Reynolds number.

CONCLUSIONS

Direct numerical simulation (DNS) of feedback control in a turbulent channel flow with a bump is performed in the present study. As the simplest feedback control, the opposition control is applied. We can achieve the total drag reduction by the control, and the drag reduction rate is found to be nearly unchanged from that in the case without a bump. It is also found that the control effect on the pressure drag is hardly observed. Furthermore, in order to investigate the dependence of the drag reduction effect on the bump height, DNS is performed in the case where the bump height is doubled. Although the total drag reduction can be achieved also in the case of $h^+ \approx 40$, it is smaller than that in the case of $h^+ \approx 20$ due to stronger flow separation and larger pressure drag. In addition, in order to investigate the Reynolds number effect of the control, we apply the control to a flow at a higher Reynolds number, i.e., $\mathrm{Re}_b = 12600$. The total drag reduction rate at $\mathrm{Re}_b = 12600$ is smaller than the case at $\mathrm{Re}_b = 5600$, and the difference of local drag reduction rate can be observed.

In the future, we will clarify a general relationship between the local pressure gradient and the local drag reduction rate to obtain more universal knowledge on the flow control effect in practical boundary layer flows and to suggest a more effective control method.

ACKNOWLEGMENTS

Authors are grateful to Drs S. Obi, K. Ando, and T. Kawata (Keio University) for fruitful discussions. This work was supported through JSPS KAKENHI grant No. 18H03758 and 21H05007 by Japan Society for the Promotion of Science.

REFERENCES

Banchetti, J., Luchini, P. & Quadrio, M. 2020 Turbulent drag reduction over curved walls. *J. Fluid Mech.* **896**, A10.

Chang, Y., Collis, S, S. & Ramakrishnan, S. 2002 Viscous effects in control of near-wall turbulence. *Phys. Fluids* **14**, 4069–4080.

Choi, H., Moin, P. & Kim, J. 1994 Active turbulence control for drag reduction in wall-bounded flows. *J. Fluid Mech.* **262**, 75–110.

Fukagata, K., Kasagi, N. & Koumoutsakos, P. 2006 A theoretical prediction of friction drag reduction in turbulent flow by superhydrophobic surfaces. *Phys. Fluids* **18**, 051703.

Hammond, E. P., Bewley, T. R. & Moin, P. 1998 Observed mechanisms for turbulence attenuation and enhancement in opposition-controlled wall-bounded flows. *Phys. Fluids* **10**, 2421–2423.

Hunt, J. C. R., Wray, A. A. & Moin, P. 1988 Eddies, streams, and convergence zones in turbulent flows. In *Proceedings of the Summer Program*, pp. 193–208. Center for Turbulence Research.

Kametani, Y. & Fukagata, K. 2011 Direct numerical simulation of spatially developing turbulent boundary layers with uniform blowing or suction. *J. Fluid Mech.* **681**, 154–172.

Kang, S. & Choi, H. 2000 Active wall motions for skin-friction drag reduction. *Phys. Fluids* **12**, 3301–3304.

Mori, E., Quadrio, M. & Fukagata, K. 2017 Turbulent drag reduction by uniform blowing over a two-dimensional roughness. *Flow Turbul. Combust.* **99**, 765–785.